Turkish Journal of Computer and Mathematics Education Vol.12 No.14 (2021),1946– 1957
Research Article

THD Measurement and Simulation of Grid-Connected Solar PV and Wind Integrated Renewable Energy System

[1]K.SUMALATHA,[2] Dr.E.MUNEENDER
[1]Research Scholar , Department of Electrical & Electronics Engineering, University college of engineering,Kottagudem Kakatiya University
[2]Assistant Professor Department of Electrical & Electronics Engineering University college of engineering,Kottagudem Kakatiya University
email Id sumalathakala@kakatiya.ac.in emai Idemuninder@gmail.com

Abstract: This paper takes us through different objectives to make the grid-connected hybrid system work effectively. In this paper, Double-Fed Induction Generator-controlled Wind Energy System integrated with a Solar PV plant is connected to the Grid. The observed non-linear variation of solar irradiation and temperature was controlled by the MPPT controller which, tries to maintain the maximum power condition at almost all instants. In this paper, the incremental conductance type MPPT method is employed for solar PV plant whereas, in the case of a wind farm, the use of back-to-back connected VSC incorporated in the DFIG maintains unity power factor for different wind speed variations. As energy availability from renewable sources is intermittent, the harmonics at the load side are inevitable. These can was reduced by using a 3-Level VSC with suitable PWM techniques to some extent. In this paper, three different cases to find the best way to integrate the wind and solar PV energy systems into the Grid have been considered. MATLAB/SIMULINK was used to do simulations with THD measurements for three different cases.

INTRODUCTION:

Energy demand is rising rapidly across the world due to modernization. At present, 80% of power to world energy is facilitating from the traditional energy sources unsafe to the atmosphere (Bhardwaj, 2018)[1][7]. Hence, there is every need to utilize renewable energy sources available that harm the atmosphere and the living organisms. In recent surveys, it is reported that by 2050 worldwide, energy demand will have tripled[11-12].

Solar PV and Wind energy incorporated systems are better choices that could be counted for fulfilling future energy needs. Despite the benefits of sustainable energy integrated systems and their reaction to underbalanced states, their performance gives preliminary results in defective grids (Shao, 2016). Various control techniques have been recommended to advance the strength of the same for superior performance in anticipation of an inoperative grid[4-5].

The primary goal of this work is to demonstrate modelling, analysis, and Total Harmonic Distortion (THD) estimation of grid-connected combined solar PV and wind energy systems. Three situations were considered in this research for the study of power system stability and power quality.

Case 1: Wind energy system linked to the Grid.

Case 2: Solar PV array system linked to the Grid.

Case 3: Integration of Solar PV and Wind Energy System as resources to the Grid.

GRID CONNECTED SOLAR PV-WIND ENERGY SYSTEM AND ITS FEATURES

Because of their abundant nature and continually decreasing investment prices, solar PV and wind energy sources are enticing electrical energy options. Wind and solar PV energy sources have a global installed capacity of more than 539 GW and 405 GW, respectively, by 2017. (Demolli, 2019). Climate conditions affect wind and PV energy sources, primarily caused by wind speed and solar irradiation. As shown in Figs. 3 and 4, a Power wind turbine (PWT) can was calculated using data of wind speed data and power curves. In the range of cut-in and rated wind speed values, the output power is non-linear and non-zero (Esteban, 2010). The power generated is not consistent in certain situations, and it may be less than the power

demand[3-6]. As a result, it must be combined with other energy sources to ensure continuous power delivery to end-users. As illustrated in Fig. 7, the output power of solar PV cells is computed based on the cell's I-V characteristics. Because Voc and Isc are primarily dependent on solar irradiance and PV cell temperature, solar PV power plants provide fluctuating power. As a result, standalone solar PV power plants were not recommended for sensitive loads that require a constant and uninterrupted power supply (Subarto Kumar Ghosh1, 2013). (El-Ghonemy, 2012)[8-10].

A.Wind energy system linked to grid.

In Figure 1, a nine-megawatt wind farm with six wind turbines each rated at 1.5 MW and linked to a 25 kV distribution grid supplies power to a 120 kV grid over a 25 kV feeder spanning over 5km and14km.

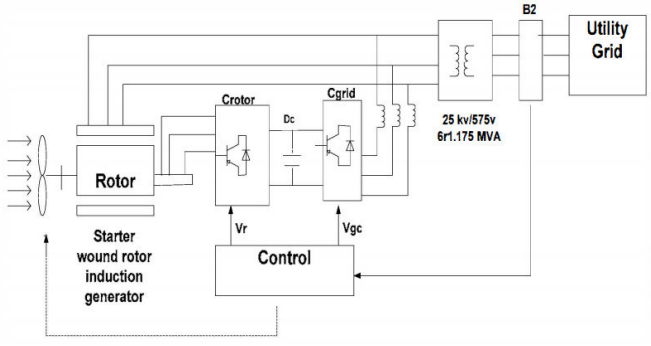

Fig.1 Grid ConnectedWindEnergy System

The Stator windings are directly connected to the transmission grid, while the rotor is at variable frequencies through theAC/DC/ACconverter.Wind turbines utilize double fed induction generators (DFIG) to create the rotor voltage and torque.DFIG extracts the maximum energy from the wind even for low wind speeds by optimizing the turbine speed while minimizing mechanical stress on the turbine. The doubly-fed induction generator-based WES mainly consists of a generator, RSC, wind turbine with the drive train system, DC-link capacitor, GSC, coupling transformer, pitch controller, and protection system. Stator of the doubly-fed induction generator is directly connected to the Grid, and rotor is coupled to the mains through an AC/DC/AC converter that only handles about 25-30% of the total power to carry out full control of the generator.. The principle of variable speed generator was obtained with the combination of DFIG, and four-quadrant AC/DC/AC VSC provided with IGBTs. The AC/DC/AC converter system contains an RSC and a GSC linked back-to-back by a DC link capacitor. RSC to change the machine excitation and electro-magnetic torque. The operation of the power converter in bidirectional power modes enables DFIG to work either in sub-synchronous or in super-synchronous operating modes. Table-1 provides the parameters of the DFIG (Nain2, 2017).

Table.1: Parameters of the DFIG

Rated power	6*1.5=9MW
Stator frequency	60Hz
Stator nominal voltage	575V
Stator resistance	0.023pu
Rotor resistance	0.016pu
Stator inductance	0.18pu
Rotor inductance	0.16pu
Inertia constant	0.685pu
Nominal DC bus voltage	1150 V

MODEL OF DFIG

A fourth-order state-space model indicates the variation of the doubly-fed induction generator through a synchronously rotating reference frame (d-q frame).

A. Control of DFIG-based WECS

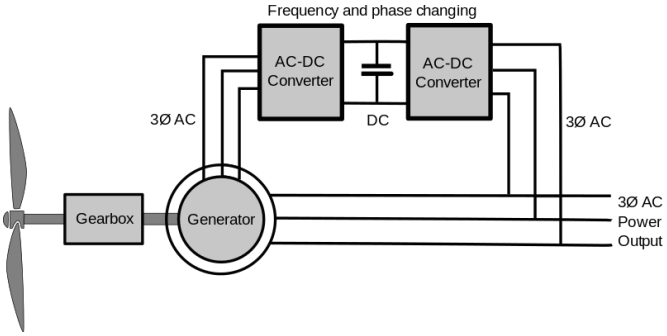

Fig.2 Block diagram of DFIG-based WECS

A control block diagram of DFIG-based WECS with two levels of control is illustrated in figure 2.
1. One of the levels is the maximum level which is WECS optimization. In this, adjusted the speed of the wind turbine such that it can obtain the optimum wind power. This control level is mechanical system control.
2. Second is the lower-level control electrical system control, i.e., torque and reactive power control.

When compared to the electrical control system, the mechanical control method is slower. Fig. 3 can show The Cp curves for wind turbines can be demonstrated in Fig. 3. The variation of turbine power, the tip speed ratio (lambda, λ) and the Cp values, with wind speed, is made evident in Fig.4.It can be seen that, for a wind speed of 15 meters per second, the output power of the turbine is 1 per unit, the pitch angle is 5.7 degrees, and the speed of the generator is 1.2 per unit.

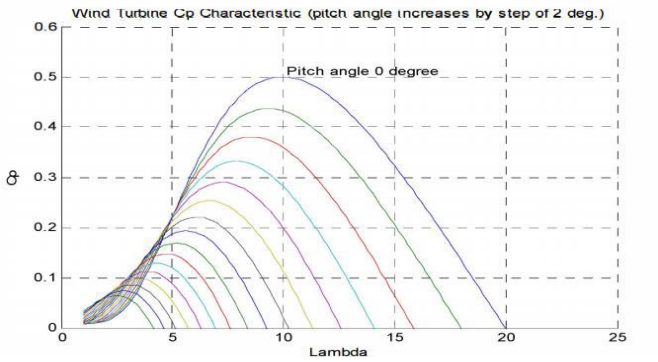

Fig.3: Pitch angle for wind turbines (increases for each step of 2 degrees)

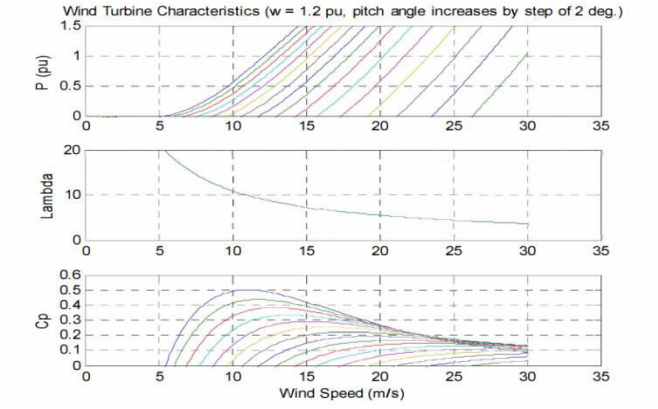

Fig.4: Wind Turbine C_p Characteristic (ω=1.2 pu. pitch angle increased by a step of 2 degree)

B. PV array system connected to grid:

Figure 5 depicts a 100-kW array connected to a 25-kV distribution grid. At 1000 W/m2 sun irradiance, the PV array can produce up to 100 kW. The voltage is raised from PV natural voltage (272 V DC at maximum power) to 500 V DC by a boost converter working at 5 kHz, with the MPPT controller enhancing the switching duty cycle of the converter. The Incremental Conductance plum is used in this controller.The Incremental Conductance with Integral Regulator technique is used in this controller. At unity power factor, the VSC transforms the available 500 V DC to 260 V AC.

A capacitor-bank advantage of 10 kVAr to filter harmonics create by Voltage Source Converter (VSC), a 100 kVA, 260 V/25kV three-phase coupling device that drives a machine is working. The utility grid model (25kV classification feeder + 120 kV equivalent transmission arrangement), B1, the grid side bus and B25, the load side transport, is proved in Fig.6. A PV array consists of abundant series and parallels linked PV modules, while a distinct PV module contains various series-connected solar cells.

The general equating that defines the I-V characteristics of an ideal cell is:

$$I_d = I_{sat}\,[e^{\mathrm{Vd/VT}} - 1] \qquad (1)$$

$$V_T = \mathrm{k}\,\frac{T}{qQ_dN_{cells}} \qquad (2)$$

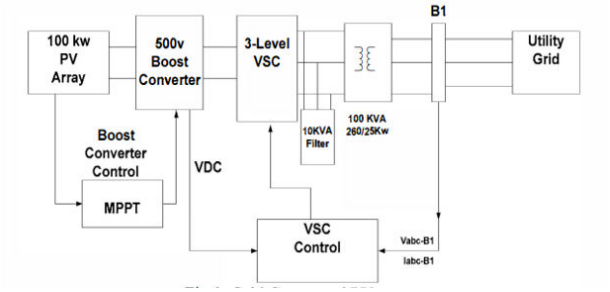

Fig.5: PV connected to Grid

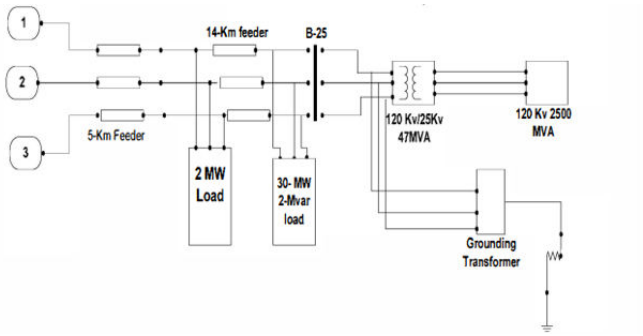

Fig.6: Utility Grid

Where,

I_d : represents the diode current.

I_{sat} : represents saturation current of the diode.

Vd : represents voltagethe diode.

VT : represents the temperature voltage.

k :represents the Boltzmann's constant value.

q :represents charge of the electron.

Q_d : represents quality factor the diode.

N_{cells}: represents the number of series connected cells per module

Iph represents the single module light photo-current generated.

The value of current generated rises in direct proportion to the solar irradiation on the module's surface as the number of parallel module strings rises. For a PV array with sixty six parallel strings (Npar) consisting of five modules (Nser) each, Equation (1) is altered to:

$I_{darray} = I_{satarray}[e^{\mathrm{Vd/Vtarray}} -1]$ (3)

Where I_{darray} is the aggregated diode current for the PV array, I_{sat} array is the aggregated diode saturation current, and V_{Tarray} is the aggregated temperature voltage. These values, along with the increased photo-current values, are $I_{pharray}$calculated as:

$I_{pharray} = I_{ph}$ X N_{par}(4)$I_{satarray} = I_{sat}$ X N_{par}(5)$V_{T\,array}$=V_T*N_{ser} (6)

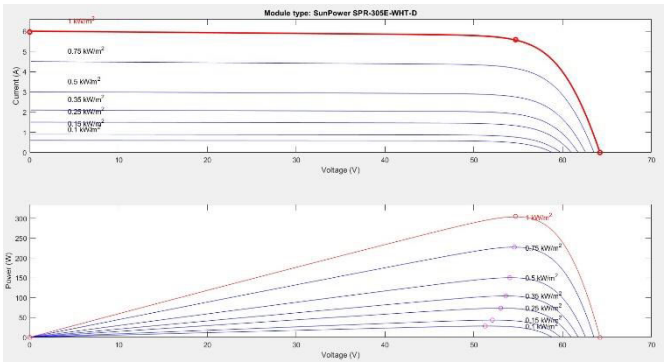

Fig.7 I-V and P-V characteristics of PV array

In Fig. 7, the dotted plots indicate deferential values of input irradiances (25 degrees Celsius, 100 W/m2). The circle underlined on the plots represents the extreme or maximum PowerPoint, and the dotted plots indicate reverent of input irradiance values (25 degrees Celsius, 100 W/m2). Table 2 shows the parameters of the sun power SPR350-WHT PV array.

Determined power for a single PV array (watt) is therefore given by:

$P_{array} = N_{par}\ X\ N_{ser}\ X\ P_{mp}$ (7)

From (7)P_{array} = 100.7 kW

Table2:SunPower SPR-305-WHT PV array Specifications

Parameter	Variable(units)	Value
Number of cells in series	N_{cells}	96

Number of series linked modules per string	N_{ser}	5
Number of parallel strings	N_{par}	66
Maximum power	P_{mp}(W)	305.2
Maximum power voltage	V_{mp}(V)	54.70
Maximum power current	I_{mp}(A)	5.58
Voltage Value of Open-circuit	V_{oc}(V)	64.20
Voltage Value of Short-circuit current	I_{sc}(A)	5.96
Voltage Value of Series connected resistance	$R_s(\Omega)$	0..0380
Voltage Value of Parallel connected resistance	$R_p(\Omega)$	993.5
Diode saturation current	I_{sat}(A)	3.1949e-8
Light generated photo-current	I_{ph}(A)	5.9602
Diode quality factor	Q_d	1.3

C. Combination ofsolor PV system and wind as hybrid sources to the grid.

Figure 8 shows the integration of a 100 kW PV array (BI Bus) and a 9 Mega Watts wind farm with six 1.5 Mega Watts wind turbines coupled to a 25-kV grid (B2 Bus).

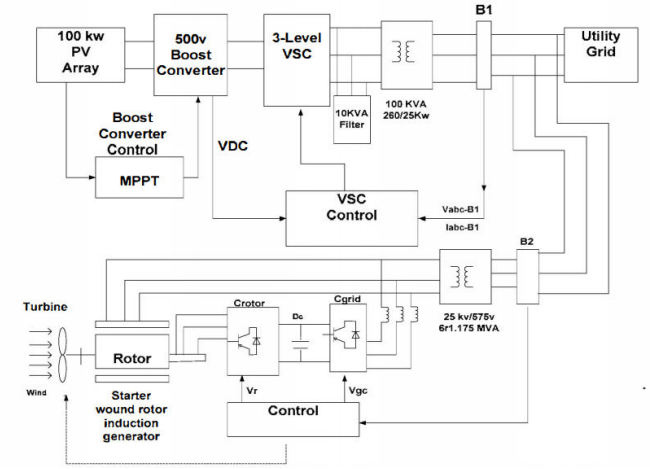

Fig.8: Integration model ofPV system and wind as hybrid sources to the grid (S. B. Mohod, 2018)

SIMULATION

Wind energy system linked to grid

The model wind speed is kept constant at 15 m/s during the first run. The DFIG (dual-fed induction generator) wind farm produces 9MW. The turbine speed is 1.2 times the synchronous generator speed. They controlled the wind turbine's reactive power at 10Mvar and regulated the DC voltage at 1150V.

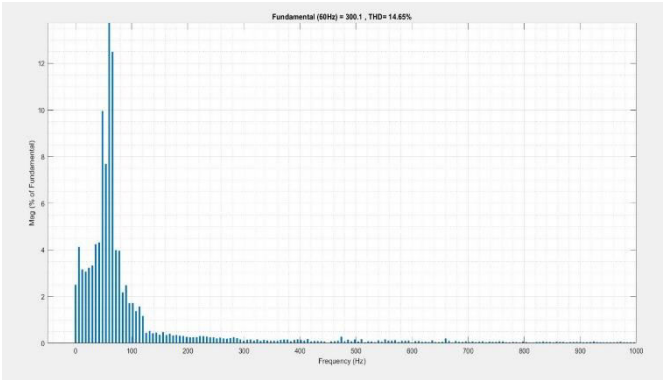

Fig. A.5: Grid side bus (B_2) THD

PV array system connected to grid

Pulses to the Boost and VSC converters are restricted from t=0 sec to t=0.05 sec when the model run for 0.7 seconds. PV voltage is similar to 321 V open-circuit voltage. The three-level bridge acted as a diode rectifier and charged the DC link capacitors to over 500 volts. The Boost and VSC converters are de-blocked at t=0.05 sec. Vdc=500V is used to manage the DC link voltage. Fixed the boost converter's duty cycle was selected (D=0.5), and the sun's irradiance was set to 1000 W/m2. At t=0.25 sec, reached the steady-state PV voltage is 250V as a result. The PV array output power is 96 kW, with a maximum capacity of 100.7 kW at 1000 W/m2 irradiance. MPPT is allowed at t=0.04 sec. The MPPT regulator begins regulating PV voltage by varying the duty cycle to extract the maximum amount of power. When the duty cycle is D=0.0453, the maximum power (100.7 kW) is obtained. PV mean voltage 274 V at t=0.5 sec, as expected given PV module specifications of 273.5V. Various irradiance adjustments are applied from t=0.5 sec to 0.7 sec to

demonstrate the MPPT controller's good performance: DC (boost converter voltage) and Mod. An index is shown in Figure A. PV array voltage boost 500V at t=0.2, and Mod. An index is 0.85.

Fig.B.1: Voltage and current from PV array different irradiations

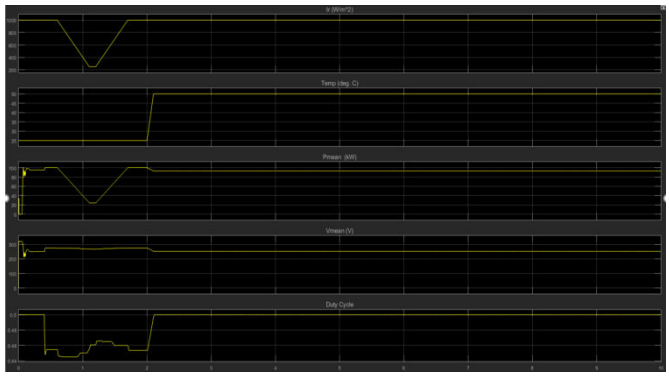

Fig.B.2: Variation of temperature, solar irradiation and duty cycle of boost converter

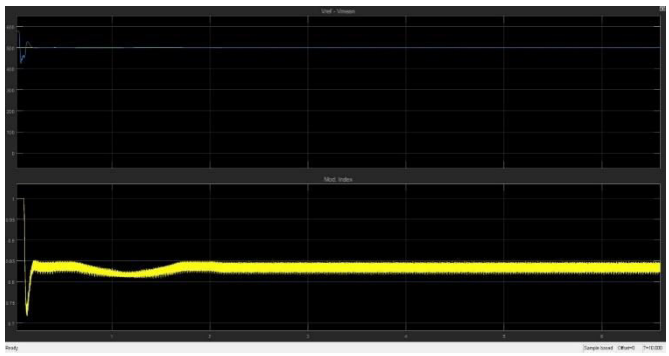

Fig. B.3: V_DC voltage(500v), Mod-index and id,iq graphs

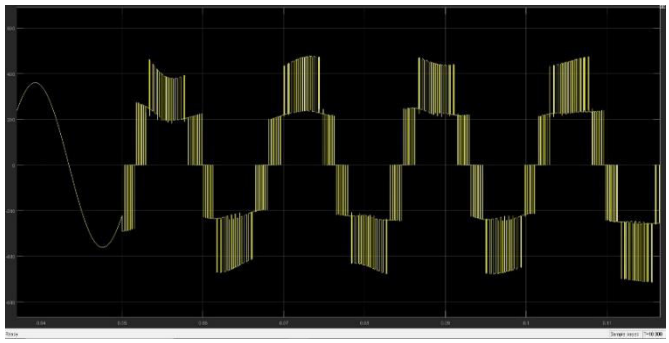

Fig.B.4: Output of three-level VSC

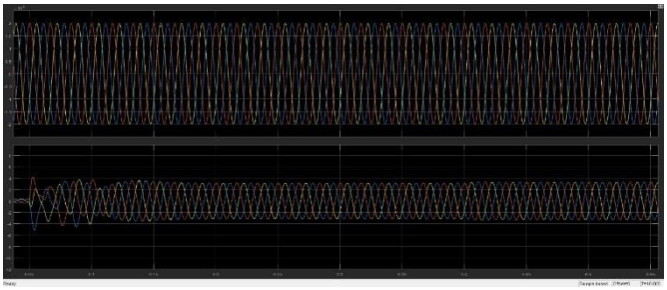

Fig. B.5: Grid side Bus B1V_abc, I_abc

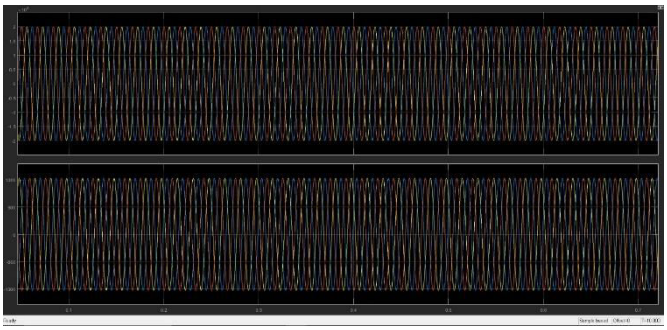

Fig. B.6: Load side bus B_25 Vabc, Iabc

The voltages and currents of the grid side bus (B 1) and load showed side bus (B 25) in Fig.B(5-6) Current THD in both the grid side bus (B 1 bus THD= 26.09%) and the load side bus (B 25 THD= 0.11%).

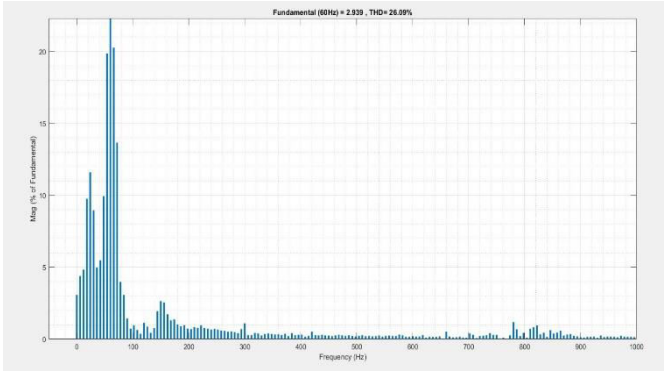

Fig. B.7: THD of Bus 1 (B_1)

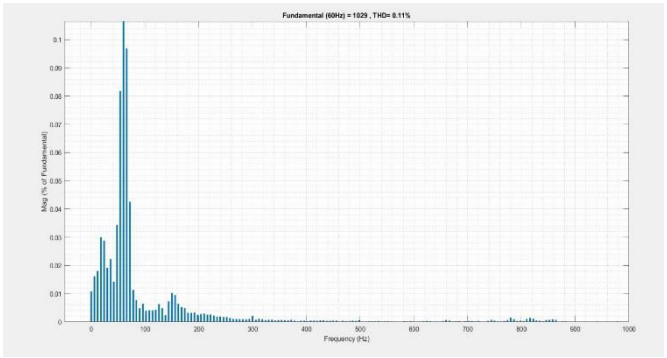

Fig. B.8: THD of Bus 25 (B _25)

A. *Integration of PV system and wind as hybrid resources to the grid*

Simulation study and THD measurement, the capacity of current and voltage of B_1bus, B_2 bus and B_25 bus shown in Fig. C(1-3). The THD of current of B_1 bus is 58.64%, B_2 bus is 18.10% and B_25 bus is 0.16% shown in Fig. C(4-6).

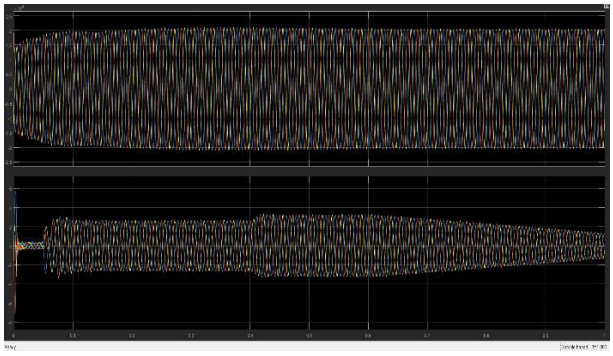

Fig. C1: Vabc and Iabc of Bus B_1

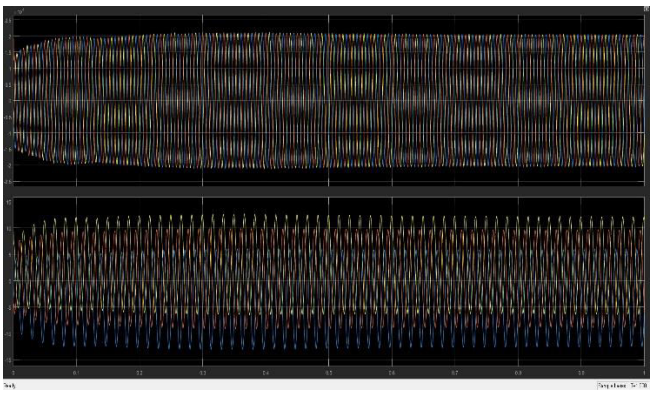

Fig. C(2): Vabc and Iabc of Bus B_2

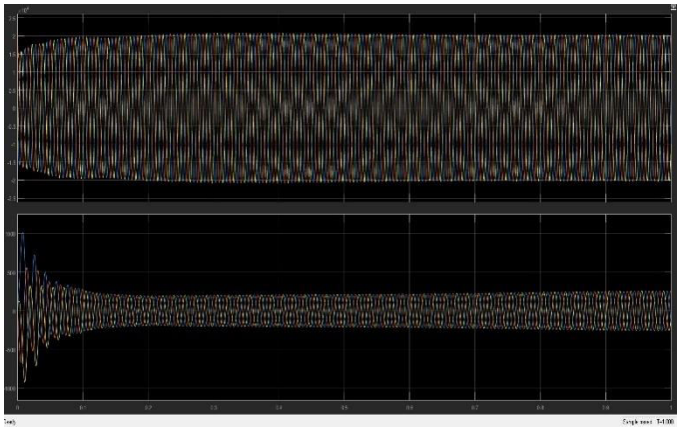

Fig.C(3): Vabc and Iabc of load side Bus B_25

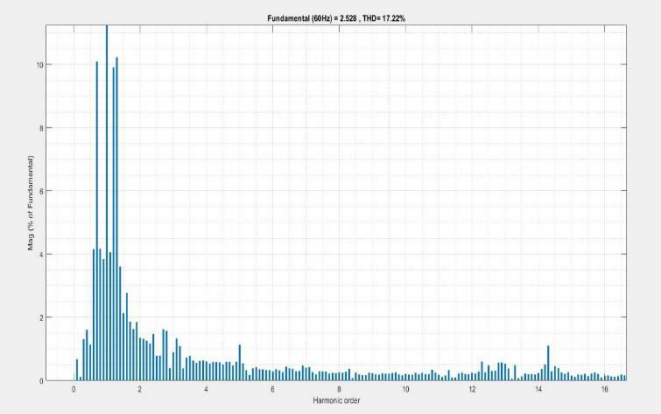

Fig.C(4): THD of BUS B_1

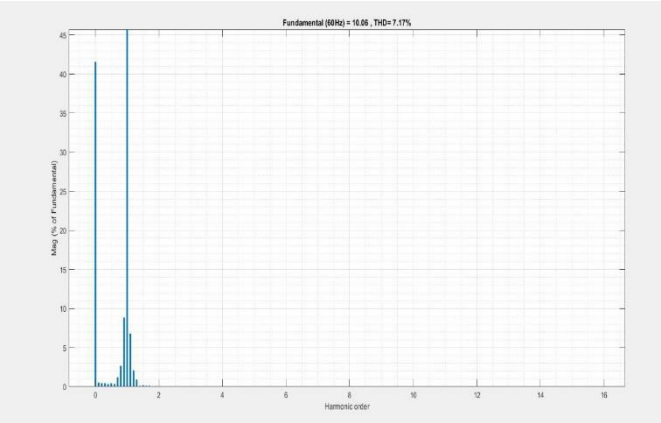

Fig.C(5): THD of Bus B_2

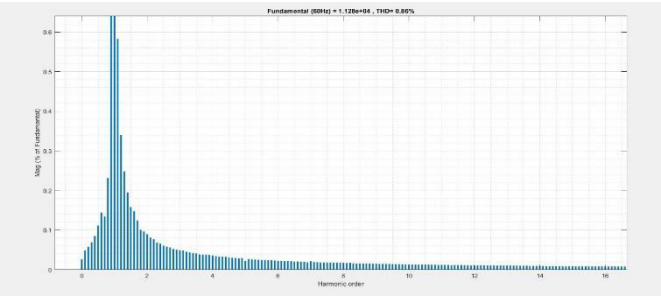

Fig.C(6): THD of load side Bus B_25

Table3: Comparison of THD values of current for different cases

	Case A	Case B	Case C
B_1 Bus	26.09	-	17.22
B_2 Bus	-	14.65	7.17
B_25 Bus	0.11	5.58	0.86

As seen in Table3, the THD of Case C is the lowest when compared to Case A, and Case B. THD lowered from Case A (B 1 Bus) to Case C (B 1 Bus) from 26.09 to 17.22, and from Case B (B 2 Bus) to Case C (B 2

Bus) from 14.65 to 7.17. THD decreased from 5.58 to 0.86 in B 25 BUS (load side bus) Case B to Case C but grew from 0.11 to 0.86 in Case A to Case C.

CONCLUSION

The DFIG and PV energy transformation system integrated with the Grid had been favourably simulating using MATLAB. The different three cases are measured to study the outcomes and determine the present THD. The system has been tested under a variety of PV irradiation conditions as well as boost converter voltage. In comparison to Case A and Case B, Case C has the lowest THD. THD reduced from Case A (B _1 Bus) to Case C (B 1Bus) from 26.09 to 17.22, and from Case B (B 2 Bus) to Case B (B 2 Bus) from 14.56 to 7.17. THD reduced 5.58 to 0.86 in the B 25 Bus (load side bus) in Case B to Case C, but improved 0.11 to 0.86 in Case A to Case C.

REFERENCES

1. Bhardwaj, S. (2018). Bhardwaj, S. *the future of public policy*
2. Demolli, H. &. (2019). *Wind power forecasting based on daily wind speed data using machine learning algorithms*
3. El-Ghonemy, A. (2012). *Photovoltaic Solar Energy: Review. International Journal of Scientific & Engineering Research.*
4. Esteban, M. &. (2010). *Esteban, Miguel & Zhang, Qi & Utama, Nuki Agya & Tezuka, Tetsuo & Ishihara, Keiichi. (2010). Methodology to estimate the output of a dual solar-wind renewable energy system in Japan. Energy Policy. 38. 7793-7802. 10.1016/j.enpol.2010.08.039.*
5. Er. Naresh Kumar, OITM HISAR; Er. Pardeep Nain, OITM HISAR (2017). *Stability Analysis of Wind Farm Based on DFIG by STATCOM.IJSRD - International Journal for Scientific Research & Development*, 5-6.
6. S. B. Mohod, V. R. (2018). *"Hybrid power system with integration of wind, battery and solar PV system,". IEEE.*
7. Shao, G. N. (2016). *Renewable and sustanable energy reviews. 139-150.*
8. Subarto Kumar Ghosh1, M. H. (2013). Modeling of PV Array and Analysis of Different Parameters. *International Journal of Advancements in Research & Technology*.
9. Praveen P., Shaik M.A., Kumar T.S., Choudhury T. (2021) Smart Farming: Securing Farmers Using Block Chain Technology and IOT. In: Choudhury T., Khanna A., Toe T.T., Khurana M., GiaNhu N. (eds) Blockchain Applications in IoT Ecosystem. EAI/Springer Innovations in Communication and Computing. Springer, Cham. https://doi.org/10.1007/978-3-030-65691-1_15
10. Praveen., P and Ch. JayanthBabu. "Big Data Clustering: Applying Conventional Data Mining Techniques in Big Data Environment." (2019).Innovations in Computer Science and Engineering, Lecture Notes in Networks and Systems 74, ISSN 2367-3370, https://doi.org/10.1007/978-981-13-7082-3_58 Springer Singapore.
11. R Ravi Kumar MBabu Reddy P Praveen, "An Evaluation Of Feature Selection Algorithms In Machine Learning" International Journal Of Scientific & Technology Research Volume 8, Issue 12, December 2019 ISSN 2277-8616,PP. 2071-2074.
12. B. Rama, P. Praveen, H. Sinha and T. Choudhury, "A study on causal rule discovery with PC algorithm," 2017 International Conference on Infocom Technologies and Unmanned Systems (Trends and Future Directions) (ICTUS), Dubai, 2017, pp. 616-621.doi: 10.1109/ICTUS.2017.8286083.